Ephemeris Closed-Loop Tracking of LEO Satellites with Pseudorange and Doppler Measurements

Nadim Khairallah and Zaher M. Kassas
University of California, Irvine

BIOGRAPHIES

Nadim Khairallah is a Ph.D. student in the Department of Mechanical and Aerospace Engineering at the University of California, Irvine and a member of the Autonomous Systems Perception, Intelligence, and Navigation (ASPIN) Laboratory. He received a B.E. in Mechanical Engineering with High Distinction from the American University of Beirut. His research interests include satellite-based opportunistic navigation and estimation theory.

Zaher (Zak) M. Kassas is an associate professor at the University of California, Irvine and director of the Autonomous Systems Perception, Intelligence, and Navigation (ASPIN) Laboratory. He is also director of the U.S. Department of Transportation Center: CARMEN (Center for Automated Vehicle Research with Multimodal AssurEd Navigation), focusing on navigation resiliency and security of highly automated transportation systems. He received a B.E. in Electrical Engineering from the Lebanese American University, an M.S. in Electrical and Computer Engineering from The Ohio State University, and an M.S.E. in Aerospace Engineering and a Ph.D. in Electrical and Computer Engineering from The University of Texas at Austin. He is a recipient of the 2018 National Science Foundation (NSF) Faculty Early Career Development Program (CAREER) award, 2019 Office of Naval Research (ONR) Young Investigator Program (YIP) award, 2018 IEEE Walter Fried Award, 2018 Institute of Navigation (ION) Samuel Burka Award, and 2019 ION Col. Thomas Thurlow Award. His research interests include cyber-physical systems, estimation theory, navigation systems, autonomous vehicles, and intelligent transportation systems.

ABSTRACT

A framework for refining the ephemerides of low Earth orbit (LEO) space vehicles (SVs) is presented. This framework is based on a known receiver that tracks the LEO SVs using pseudorange and Doppler measurements extracted from the LEO SVs' signals. A procedure to determine the process noise covariance for the LEO SVs' motion is developed. Monte Carlo simulations are performed to demonstrate the improvements in the tracked LEO SVs' ephemerides over open-loop SGP4-propagated ephemerides for three measurement scenarios: (i) pseudorange, (ii) Doppler, and (iii) pseudorange and Doppler. The improved ephemerides are subsequently utilized to localize an unknown receiver drawing pseudorange measurements on LEO SVs, and the resulting positioning error is compared for the true, open-loop, and closed-loop SV ephemerides. Experimental results are presented showing (i) a refinement of two Orbcomm LEO SVs' ephemerides with reductions of 879.3 m and 817.7 m in their estimated position errors over SGP4 predictions and (ii) a 53.65% reduction in the two-dimensional (2-D) localization error of an unknown stationary receiver by using the tracked ephemerides instead of SGP4-propagated ephemerides.

I. INTRODUCTION

Low Earth orbit (LEO) space vehicles (SVs) inherently exhibit advantageous characteristics for navigation as a result of their orbital properties. To maintain SVs' stable low Earth orbits, LEO SVs orbit the Earth at fast speeds, resulting in short orbital periods [1]. Being mainly used for communication and broadband Internet [2], LEO SVs' objectives are to ensure both global coverage and continuity of signals for users on Earth [3]. Low orbital altitudes lead to restricted fields of view, while the large speeds result in short periods of line-of-sight access to receivers on Earth (on the order of a few minutes) [4]. To remedy the aforementioned issues, LEO SVs designers build constellations, which are networks of multiple LEO satellites in different orbital planes [5]. In fact, many companies are launching mega-constellations [6,7], the most notable example being SpaceX which has filed with the Federal Communications Commision (FCC) for permission to launch 30,000 LEO SVs, in addition to the already approved 12,000, for their Starlink constellation [8]. With around 5,000 LEO SVs in orbit as of March 2021 [9], the LEO space race is showing no signs of slowing down in the foreseeable future [10]. This exponentially growing interest in LEO SVs with continuous

Preprint of the 2021 ION GNSS+ Conference
St. Louis, MO, September 20–24, 2021

satellite launches and even new constellations designs fuels the abundance of LEO SVs orbiting Earth. The sheer number of satellites in LEO will yield low geometric dilution of precision (GDOP), which in turn gives more precise position and velocity estimates [11]. Furthermore, the numerous constellations give also rise to spectral diversity, which improves the robustness to interference, whether unintentional or targeted (e.g. jamming), and to malicious spoofing attacks by providing information from a wider spectrum. Finally, LEO SVs are around twenty times closer to Earth than GNSS satellites residing in medium Earth orbit (MEO), which results in the received power of LEO signals being 300 to 2400 times more powerful than their GNSS counterparts [12].

To take advantage of these appealing navigation characteristics of LEO SVs, two main challenges have to be accounted for. On one hand, since these SVs are not intended for navigation, one must design receivers capable of producing navigation observables (pseudorange, carrier phase, and Doppler) from the SVs' downlink signals. Moreover, these signals are partially known or even completely unknown as the LEO SV operators are private and the information transmitted by their satellites is proprietary. On the other hand, unlike GNSS satellites in MEO that transmit their precise ephemerides in their navigation message, LEO SVs do not usually openly share knowledge about their position. The most accurate publicly-available information on LEO SVs' ephemerides are in the form of two-line element (TLE) files generated by the North American Aerospace Defense Command (NORAD), which are typically updated daily [13]. The LEO SVs' TLEs consist of a set of six mean Keplerian elements (inclination, right ascension of ascending node, eccentricity, argument of perigee, mean anomaly, and mean motion) defined at a specified epoch which fully characterize the orbit of the LEO SVs. TLE files can be propagated using the analytical Simplified General Perturbation (SGP4) model [14], but the resulting SVs' position will suffer from errors on the order of a few kilometers, which will inevitably degrade any navigation performance.

The first challenge can be addressed with the design of specialized software-defined radio (SDR) receivers that exploit the periodic signals with favorable correlation properties transmitted by LEO SVs to extract navigation observables [15–20]. Even mysterious signals can be meaningfully processed by cognitive receivers to obtain useful navigation information [21–25]. Furthermore, with the development of these receivers, code phase (pseudorange) measurements could be extractable from LEO SVs' signals in addition to Doppler (pseudorange rate) measurements.

The second challenge can be addressed by improved orbit prediction algorithms, which can be categorized into analytical and numerical [26–28]. Recently, machine learning approaches have shown great promise for improved orbit prediction [29–32]. Previous work has considered the use of simple analytical and machine learning orbit propagators into a so-called simultaneous tracking and navigation (STAN) framework, in which a vehicle-mounted receiver simultaneously estimates its own states along side the states of LEO SVs [33–36].

This paper studies improved LEO SV ephemeris tracking when a known receiver incorporates pseudorange and/or Doppler measurements to a LEO SV into its estimator, which is tracking the LEO SV. This paper makes the following four contributions. First, a framework to match the process noise covariance matrix for the SV's motion is proposed based on a Monte Carlo analysis. Although performed on randomized realizations of a single satellite for a specified reference frame and duration at a specific time, this procedure is generalized to any LEO SV by expressing the process noise covariance matrix in the SV's body frame. Second, the tracking of LEO SVs' ephemerides by a known receiver extracting observables from the SVs' signals is performed in an extended Kalman filter (EKF) using three different sets of measurements: (i) pseudoranges, (ii) Dopplers, and (iii) both pseudoranges and Dopplers. It is shown that using pseudorange measurements yield much lower LEO SV position estimation errors compared to using Doppler measurements, but the performance becomes asymptotically comparable. Moreover, it is shown that fusing pseudorange and Doppler measurements yield little reduction in the LEO SV position estimation error compared to using pseudorange measurements alone. Third, unknown receiver localization is demonstrated to assess the improvements resulting from the EKF-refined SVs' ephemerides over the open-loop SGP4-propagated ephemerides. Fourth, experimental results are presented, where a receiver with known states tracks two Orbcomm LEO SVs and hands over the improved ephemerides to a stationary receiver with an unknown position which in turn localizes itself with carrier phase measurements to these two LEO SVs. The unknown receiver is assumed to have a very poor prior about its initial position (initial position error of 1,047 km). It is shown that the 2-D localization error reduces from 1,687 m if the ephemerides are propagated through SGP4 to 782 m. It is worth noting that Orbcomm LEO SVs periodically transmit their positions, which are estimated by onboard GPS receivers. If these positions are used as "ground truth" instead of the estimated LEO SVs ephemerides, the 2-D localization error is 498 m.

The rest of the paper is organized as follows. Section II describes the LEO satellite's dynamics and the pseudorange

and Doppler measurement models. Section III discusses the procedure used to perform the closed-loop tracking of LEO SVs. Section IV shows an application of this improved LEO SV ephemeris tracking in the context of a stationary receiver localizing itself, given the improved LEO SV ephemeris. Section V shows experimental results demonstrating tracking of a LEO satellites' ephemerides and unknown receiver localization. Section VI gives concluding remarks.

II. MODEL DESCRIPTION

This section presents the LEO SVs' dynamics and the pseudorange and Doppler measurements.

A. LEO Satellite Dynamics

LEO SVs maintain their orbital motion under the action of Earth's gravitational field. This gravitational force directly translates into the following satellite's equations of motion given by

$$\ddot{\boldsymbol{r}}_{\text{sv}} = \frac{\partial U}{\partial \boldsymbol{r}_{\text{sv}}} + \tilde{\boldsymbol{w}}_{\text{sv}}, \tag{1}$$

where $\boldsymbol{r}_{\text{sv}} \triangleq [x_{\text{sv}}, y_{\text{sv}}, z_{\text{sv}}]^{\mathsf{T}}$ is the SVs' position in an Earth-centered inertial (ECI) reference frame, U is Earth's gravitational potential (geopotential) at the LEO SV, and $\tilde{\boldsymbol{w}}_{\text{sv}}$ is a vector of unmodeled acceleration perturbations expressed in the same ECI frame as the SV's position. This vector encompasses perturbing accelerations resulting from Earth's non-uniform gravitational potential unmodeled in U, atmospheric drag, solar radiation pressure, gravitational pull of other celestial bodies, and general relativity [37].

Accounting for Earth's oblateness resulting in a non-uniform gravitational field, the geopotential is modeled using the spherical harmonics representation for oblate spheroids [38]. Using satellite observations, many models have been fit to determine the zonal, sectoral, and tesseral coefficients of the spherical harmonic functions characterizing Earth's geopotential. One such model commonly used is the JGM-3 model developed by the Goddard Space Flight Center [39]. Neglecting the sectoral and tesseral coefficients as their influence is several order of magnitudes smaller than the zonal coefficients, denoted $J_n, n = 2, 3, \ldots, \infty$, the geopotential at the LEO SV is expressed as [40]

$$U = \frac{\mu}{\|\boldsymbol{r}_{\text{sv}}\|}\left[1 - \sum_{n=2}^{\infty} J_n \frac{R_E^n}{\|\boldsymbol{r}_{\text{sv}}\|^n} P_n\left(\sin(\theta)\right)\right], \tag{2}$$

where J_n is the n^{th} zonal coefficient, R_E is the mean radius of the Earth, P_n is a Legendre polynomial with harmonic n, and $\sin(\theta) = z_{\text{sv}}/\|\boldsymbol{r}_{\text{sv}}\|$.

Taking into account the first-order effect of the J_2 coefficient as the most dominant term of Earth's oblateness (second-order J_2 and J_4 effects are three order of magnitudes smaller), the equations of motion of a satellite are then derived by combining (1) and (2) to yield

$$\begin{aligned}
\ddot{x}_{\text{sv}} &= \frac{\partial U}{\partial x_{\text{sv}}} = -\frac{\mu x_{\text{sv}}}{\|\boldsymbol{r}_{\text{sv}}\|^3}\left[1 + J_2\frac{3}{2}\left(\frac{R_E}{\|\boldsymbol{r}_{\text{sv}}\|}\right)^2\left(1 - 5\frac{z_{\text{sv}}^2}{\|\boldsymbol{r}_{\text{sv}}\|^2}\right)\right] + \tilde{w}_x,\\
\ddot{y}_{\text{sv}} &= \frac{\partial U}{\partial y_{\text{sv}}} = -\frac{\mu y_{\text{sv}}}{\|\boldsymbol{r}_{\text{sv}}\|^3}\left[1 + J_2\frac{3}{2}\left(\frac{R_E}{\|\boldsymbol{r}_{\text{sv}}\|}\right)^2\left(1 - 5\frac{z_{\text{sv}}^2}{\|\boldsymbol{r}_{\text{sv}}\|^2}\right)\right] + \tilde{w}_y,\\
\ddot{z}_{\text{sv}} &= \frac{\partial U}{\partial z_{\text{sv}}} = -\frac{\mu z_{\text{sv}}}{\|\boldsymbol{r}_{\text{sv}}\|^3}\left[1 + J_2\frac{3}{2}\left(\frac{R_E}{\|\boldsymbol{r}_{\text{sv}}\|}\right)^2\left(3 - 5\frac{z_{\text{sv}}^2}{\|\boldsymbol{r}_{\text{sv}}\|^2}\right)\right] + \tilde{w}_z,
\end{aligned} \tag{3}$$

where $\tilde{\boldsymbol{w}}_{\text{sv}} \triangleq [\tilde{w}_x, \tilde{w}_y, \tilde{w}_z]^{\mathsf{T}}$ is modeled as a zero-mean white Gaussian random vector with covariance $\mathbf{Q}_{\tilde{w}_{\text{sv}}}$.

B. Measurement Models

The closed-loop tracking of LEO satellites is performed using pseudorange and pseudorange rate measurements extracted by a receiver from received LEO SVs' signals.

The pseudorange measurement $\rho(k)$ between a receiver and a LEO SV at time-step k is modeled by

$$\rho(k) = \|\boldsymbol{r}_r(k) - \boldsymbol{r}_{\text{sv}}(k)\|_2 + c \cdot [\delta t_r(k) - \delta t_{\text{sv}}(k)] + c\delta t_{\text{iono}}(k) + c\delta t_{\text{tropo}}(k) + v_\rho(k), \quad k = 1, 2, \ldots \tag{4}$$

where δt_r and δt_{sv} are the receiver's and LEO SV's clock biases, respectively; δt_{iono} and δt_{tropo} are the ionospheric and tropospheric delays, respectively; and v_ρ is the pseudorange measurement noise which is modeled as a zero-mean white Gaussian random sequence with variance σ_ρ^2.

In addition to pseudorange measurements, the receiver tracks the LEO SV's Doppler f_D, from which pseudorange rate observables can be readily calculated as $\dot{\rho} = -\frac{c}{f_c} f_D$, where c is the speed of light and f_c is the LEO SV downlink signal carrier frequency.

The pseudorange rate measurement $\dot{\rho}(k)$ between a receiver and a LEO SV at time-step k is modeled by

$$\dot{\rho}(k) = [\dot{\boldsymbol{r}}_r(k) - \dot{\boldsymbol{r}}_{\text{sv}}(k)]^{\mathsf{T}} \frac{[\boldsymbol{r}_r(k) - \boldsymbol{r}_{\text{sv}}(k)]}{\|\boldsymbol{r}_r(k) - \boldsymbol{r}_{\text{sv}}(k)\|_2} + c \cdot \left[\dot{\delta} t_r(k) - \dot{\delta} t_{\text{sv}}(k)\right] + c\dot{\delta} t_{\text{iono}}(k) + c\dot{\delta} t_{\text{tropo}}(k) + v_{\dot{\rho}}(k), \quad k = 1, 2, \ldots \tag{5}$$

where $\dot{\delta} t_r$ and $\dot{\delta} t_{\text{sv}}$ are the receiver's and LEO SV's clock drifts, respectively; $\dot{\delta} t_{\text{iono}}$ and $\dot{\delta} t_{\text{tropo}}$ are the drifts of ionospheric and tropospheric delays, respectively; and $v_{\dot{\rho}}$ is the pseudorange rate measurement noise which is modeled as a zero-mean white Gaussian random sequence with variance $\sigma_{\dot{\rho}}^2$.

III. LEO SV Tracking

This section formulates the ephemeris closed-loop LEO SV tracking framework with pseudorange and Doppler measurements. Monte Carlo simulations are presented comparing the tracking performance of SGP4 versus that with pseudorange, Doppler, and fused pseudorange and Doppler measurements.

A. Process Noise Covariance Determination

Since the process noise covariance matrix $\mathbf{Q}_{\text{sv}}$ not only affects the uncertainty propagation, but also directly impacts the states' estimates in the EKF, it is of critical importance to accurately characterize $\mathbf{Q}_{\text{sv}}$ before implementing the closed-loop tracking of LEO SVs. To accomplish this, a framework is developed based on Monte Carlo simulations as follows:

1. A NORAD-generated publicly available two-line element (TLE) reference file is selected for an Orbcomm LEO SV. The reference TLE epoch as well as the the six mean Keplerian elements given at this TLE epoch (inclination, right ascension of ascending node, eccentricity, argument of perigee, mean anomaly, and mean motion) fully define the orbit of the Orbcomm SV. This reference TLE is propagated for one orbital period of duration $K = 6000$ seconds with a time-step of one second using the SGP4 propagator and the predicted SV position and velocity is denoted by $\boldsymbol{x}_{\text{SGP4},ref}(k),\ k = 1, 2, \ldots, K+1$.
2. N Monte Carlo realizations are created by drawing samples from a Gaussian distribution centered at the reference TLE mean Keplerian elements with a specified covariance matrix that emulates the TLE files' uncertainty at epoch. For each of these N realizations, a TLE file is generated with the same epoch as the reference TLE but with the randomized mean Keplerian elements.
3. Each of the N randomized TLE realizations of the reference TLE are propagated for $K = 6000$ seconds with a time-step of one second using the SGP4 propagator and the predicted SV position and velocity $\boldsymbol{x}_{\text{SGP4},i}(k)$ are stored at each time-step k for each realization i, where $k = 1, 2, \ldots, K+1$ and $i = 1, 2, \ldots, N$.
4. For each Monte Carlo realization i, the value of the process noise $\boldsymbol{w}_i$ is calculated at each time-step k according to $\boldsymbol{w}_i(k) = \boldsymbol{x}_{\text{SGP4},i}(k+1) - \boldsymbol{f}\left(\boldsymbol{x}_{\text{SGP4},i}(k)\right)$, where $\boldsymbol{f}$ is the nonlinear SV dynamics propagation model used in the filter's prediction step.
5. The empirical covariance $\mathbf{Q}_{\text{emp}}$ of the process noise is computed at each time-step k by averaging $\boldsymbol{w}_i(k)\boldsymbol{w}_i^{\mathsf{T}}(k)$ across Monte Carlo realizations according to $\mathbf{Q}_{\text{emp}}(k) = \frac{1}{N}\sum_{i=1}^{N} \boldsymbol{w}_i(k)\boldsymbol{w}_i^{\mathsf{T}}(k)$.

Since both the SGP4 propagation $\boldsymbol{x}_{\text{SGP4},i}(k+1)$ and the filter's prediction $\boldsymbol{f}\left(\boldsymbol{x}_{\text{SGP4},i}(k)\right)$ are performed in the ECI reference frame, the values of the process noise for each realization $\boldsymbol{w}_i(k)$ are also vectors in the ECI frame. As a result, $\mathbf{Q}_{\text{emp}}(k)$ will be the empirical process noise covariance at each time-step expressed in the ECI frame.

To provide a more intuitive interpretation of the effect of the process noise on the LEO SV's motion, the rotation matrix from the ECI frame to the SV's body frame (along-track, cross-track, and radial directions) ${}^{b}_{e}\mathbf{R}$ is computed at each time-step k and the empirical process noise covariance determined by the Monte Carlo analysis described above $\mathbf{Q}_{\text{emp}}(k)$ is rotated to form $\mathbf{Q}_{\text{emp},body}(k),\ k = 1, 2, \ldots, K+1$.

In addition to providing a more intuitive and visual interpretation of the process noise, $\mathbf{Q}_{\text{emp},body}$ is also more invariant than $\mathbf{Q}_{\text{emp}}$ since in the SV's body frame, the satellite's motion is constrained to be in the along-track – radial plane (orbital plane) with the velocity in the along-track direction and with no motion in the cross-track direction; whereas in the ECI frame, the LEO SV's motion has generally components in all directions which are time-varying as the satellite orbits Earth. Moreover, the invariance brought by the expression of the process noise covariance matrix in the SV's body frame allows for a generalization of $\mathbf{Q}_{\text{emp},body}$ to all LEO SVs, which have similar motion characteristics in the body frame, while $\mathbf{Q}_{\text{emp}}$ would only be applicable for the reference SV chosen in the Monte Carlo analysis at a specific time determined by the satellite's position in the ECI frame. To further enhance the generalization of the process noise covariance matrix, the invariance of $\mathbf{Q}_{\text{emp},body}$ is leveraged to define $\bar{\mathbf{Q}} \triangleq \frac{1}{K}\sum_{k=1}^{K} \mathbf{Q}_{\text{emp},body}(k)$, which will be used in the LEO SV tracking filter. The uncertainty ellipse associated with $\bar{\mathbf{Q}}$ can be visualized in Fig. 1.

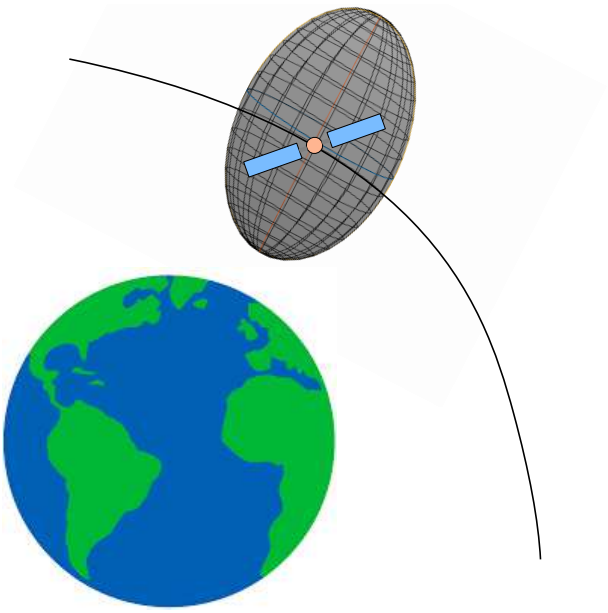

Fig. 1. Visualization of the 95% error ellipse of the averaged process noise covariance characterized for one orbital period in the body frame for the LEO SV position states.

Fig. 2 shows the difference between (i) the empirical covariance matrix $\mathbf{P}_{\text{emp}}(k) = \frac{1}{N}\sum_{i=1}^{N} \tilde{\boldsymbol{x}}_i(k)\tilde{\boldsymbol{x}}_i^{\mathsf{T}}(k)$, where $\tilde{\boldsymbol{x}}_i(k) \triangleq \boldsymbol{x}_{\text{SGP4},i}(k) - \boldsymbol{x}_{\text{SGP4},ref}(k)$, computed from the Monte Carlo runs of SGP4 propagation of the different TLE realizations and rotated to the body frame and (ii) the open-loop filter propagation of the initial empirical covariance matrix $\mathbf{P}_{\text{emp}}(1)$ in the body frame using $\bar{\mathbf{Q}}$ to account for the process noise of the SV's position and velocity states.

Finally, note that the time-step of one second used in the above procedure to determine the process noise covariance matrix is the same as the filter's propagation horizon in Sections III-B and V. This fact justifies the use of $\bar{\mathbf{Q}}$ rotated to the ECI frame as the process noise covariance matrix of the filter.

B. Ephemeris Closed-loop Tracking

The closed-loop tracking of a LEO SV is performed by an EKF that recursively performs a measurement update whenever a new measurement becomes available. The state vector estimated by the EKF is defined as $\boldsymbol{x} \triangleq \left[\boldsymbol{r}_{\text{sv}}^{\mathsf{T}}, \dot{\boldsymbol{r}}_{\text{sv}}^{\mathsf{T}}, c\Delta\delta t_{\text{sv}}, c\Delta\dot{\delta} t_{\text{sv}}\right]^{\mathsf{T}}$, where $\boldsymbol{r}_{\text{sv}}$ and $\dot{\boldsymbol{r}}_{\text{sv}}$ are the LEO SV's position and velocity in an ECI reference frame respectively, $c\Delta\delta t_{\text{sv}} \triangleq c \cdot [\delta t_r - \delta t_{\text{sv}}]$ is the difference between the receiver's and LEO SV's clock biases, and

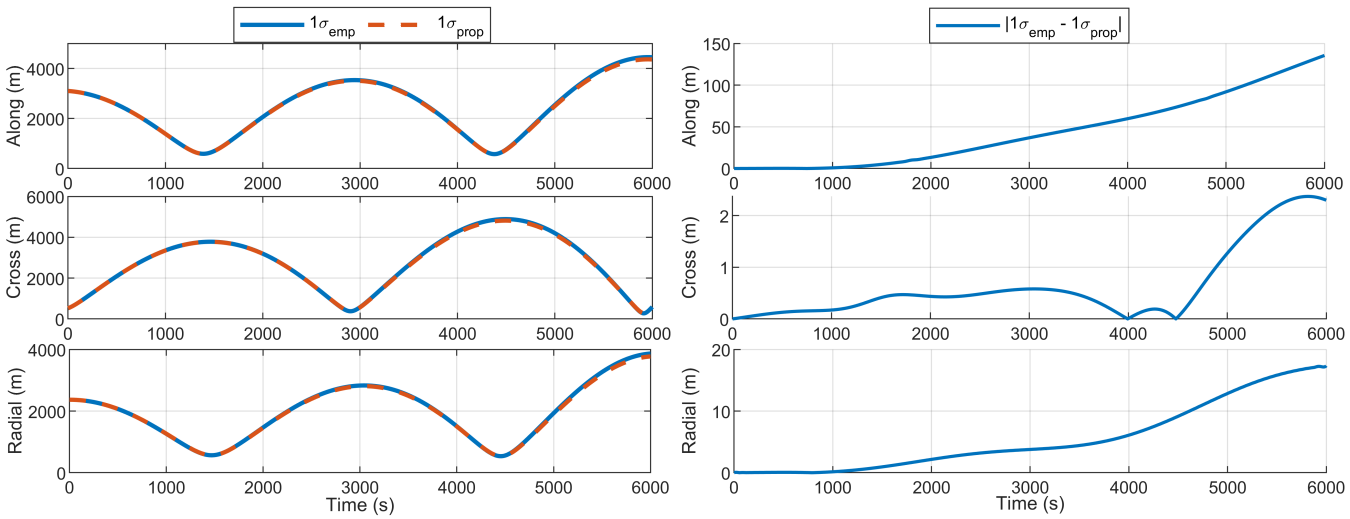

Fig. 2. Empirical and propagated standard deviations for the LEO SV position states in the body frame (left) and absolute difference between them (right) over one orbital period (100 minutes).

$c\Delta\dot{\delta}t_{\text{sv}} \triangleq c \cdot \left[\dot{\delta}t_r - \dot{\delta}t_{\text{sv}}\right]$ is the difference between the receiver's and LEO SV's clock drifts.

The EKF state and covariance time updates are given by

$$\hat{\boldsymbol{x}}(k+1|k) = \boldsymbol{f}\left(\hat{\boldsymbol{x}}(k|k)\right), \qquad \mathbf{P}(k+1|k) = \mathbf{F}(k)\mathbf{P}(k|k)\mathbf{F}^{\mathsf{T}}(k) + \mathbf{Q}(k), \tag{6}$$

where $\boldsymbol{f}$ is the nonlinear SV dynamics obtained by numerical integration of the SV dynamics (3), $\mathbf{F}(k) \triangleq \frac{\partial \boldsymbol{f}}{\partial \boldsymbol{x}}\big|_{\hat{\boldsymbol{x}}(k|k)}$ is the Jacobian of $\boldsymbol{f}$ linearized about $\hat{\boldsymbol{x}}(k|k)$, and $\mathbf{Q}(k)$ is the process noise covariance matrix, readily calculated by rotating $\bar{\mathbf{Q}}$ determined in Section III-A to the ECI frame in which the filter runs by applying ${}^{e}_{b}\mathbf{R}(k)$, the rotation matrix from the body frame to the ECI frame at time-step k.

The EKF state and covariance measurement updates are given by

$$\hat{\boldsymbol{x}}(k+1|k+1) = \hat{\boldsymbol{x}}(k+1|k) + \mathbf{K}(k+1)\boldsymbol{\nu}(k+1), \qquad \mathbf{P}(k+1|k+1) = \mathbf{P}(k+1|k) - \mathbf{K}(k+1)\mathbf{H}(k+1)\mathbf{P}(k+1|k), \tag{7}$$

where $\mathbf{K}(k+1)$ is the standard Kalman gain, $\boldsymbol{\nu}(k+1) = \boldsymbol{z}(k+1) - \boldsymbol{h}(\hat{\boldsymbol{x}}(k+1|k))$ is the innovation vector, and $\mathbf{H}(k+1) \triangleq \frac{\partial \boldsymbol{h}}{\partial \boldsymbol{x}}\big|_{\hat{\boldsymbol{x}}(k+1|k)}$ is the measurement Jacobian for $\boldsymbol{z} = \boldsymbol{h}(\boldsymbol{x})$, linearized about $\hat{\boldsymbol{x}}(k+1|k)$.

To validate the tracking performance of LEO SVs, a high-fidelity simulator is used, namely Analytical Graphics Inc. (AGI) Systems Tool Kit (STK) [41] using a High-Precision Orbit Propagator (HPOP) [26]. This ephemeris data is treated as ground truth emulating the actual trajectory of an Orbcomm SV. In parallel, a TLE file for this HPOP orbit was generated in STK using 300 observations spanning 24 hours before a set epoch to solve a batch least squares problem and give the mean Keplerian element at this epoch that most closely match the true ephemeris. This procedure of generating the TLE is identical to the one used by NORAD to create the publicly-available TLEs for many space objects. The generated TLE is then propagated using SGP4 around 18.5 hours forward to the initial time of a period of line-of-sight access between a simulated known receiver and the LEO SV. The filter's states are randomly initialized around STK's ground truth with an initial covariance matrix that matches the error between the SGP4 propagated states and the ground truth at the filter's first time-step. Then, the closed-loop tracking of the LEO SV by the known receiver in an EKF with different measurements is performed and the filter's estimates are compared to STK's ground truth over the period of the SV's visibility. This simulation will be performed using 100 Monte Carlo runs and the root mean-squared error (RMSE) of the EKF tracking across realizations is compared to the open-loop SGP4 propagation errors.

When pseudoranges are used to track the LEO SV, $z = \rho$ and the measurement Jacobian $\mathbf{H}_\rho$ is formed according to $\mathbf{H}_\rho(k+1) = \begin{bmatrix} -\boldsymbol{l}_{\text{sv}}^{\mathsf{T}}(k+1) & \mathbf{0}_{1\times 3} & 1 & 0 \end{bmatrix}$, where $\boldsymbol{l}_{\text{sv}}(k+1) \triangleq \frac{[\boldsymbol{r}_r(k+1) - \hat{\boldsymbol{r}}_{\text{sv}}(k+1|k)]}{\|\boldsymbol{r}_r(k+1) - \hat{\boldsymbol{r}}_{\text{sv}}(k+1|k)\|_2}$.

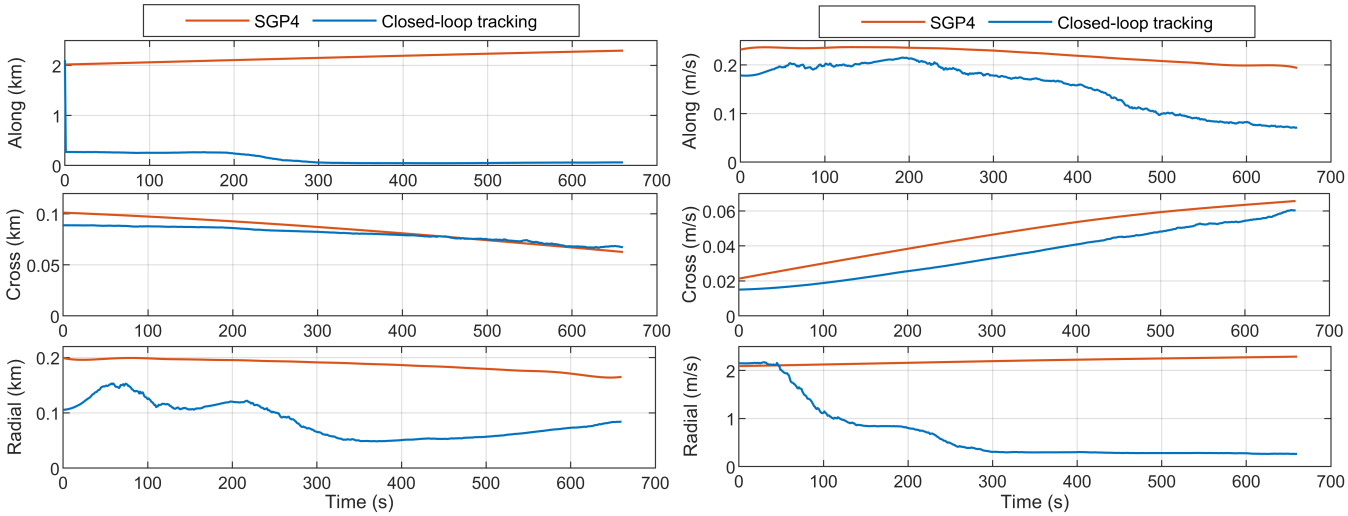

Fig. 3. LEO SV position and velocity closed-loop tracking RMSEs with pseudoranges versus SGP4 errors.

If pseudorange rates are the only measurements available to track the LEO SV, $z = \dot{\rho}$ and the measurement Jacobian $\mathbf{H}_{\dot{\rho}}$ is formed according to $\mathbf{H}_{\dot{\rho}}(k{+}1) = \left[\frac{[\dot{\boldsymbol{r}}_r(k+1)-\hat{\dot{\boldsymbol{r}}}_{\text{sv}}(k+1|k)]^{\mathsf{T}}}{\|\dot{\boldsymbol{r}}_r(k+1)-\hat{\dot{\boldsymbol{r}}}_{\text{sv}}(k+1|k)\|_2}\left[\boldsymbol{l}_{\text{sv}}(k+1)\boldsymbol{l}_{\text{sv}}^{\mathsf{T}}(k+1) - \mathbf{I}_{3\times 3}\right] \quad -\boldsymbol{l}_{\text{sv}}^{\mathsf{T}}(k+1) \quad 0 \quad 1\right]$.

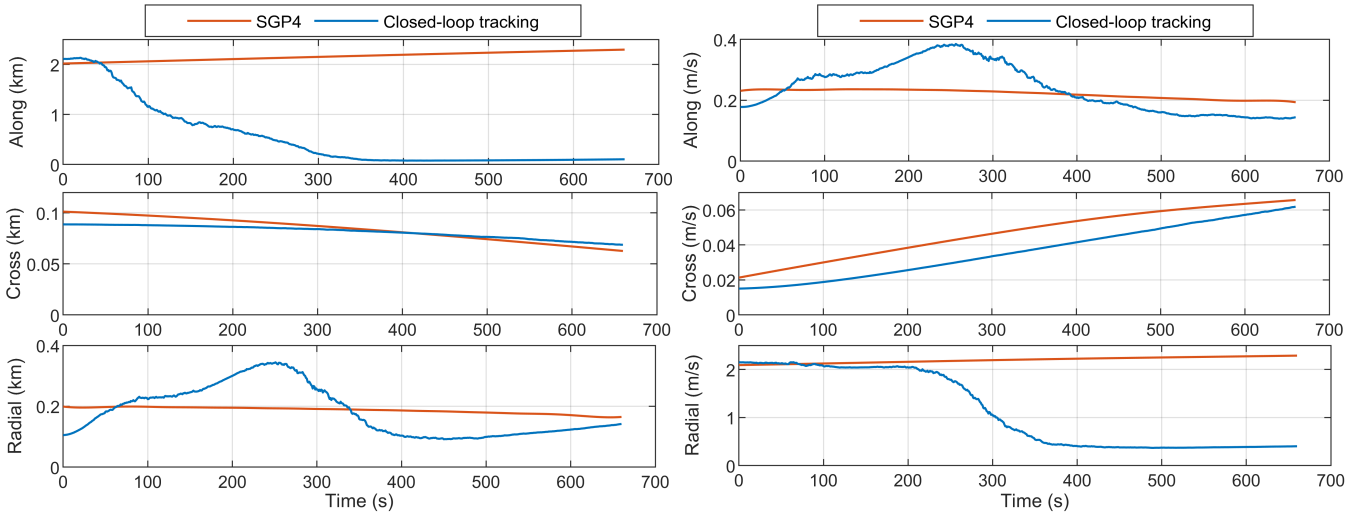

Fig. 4. LEO SV position and velocity closed-loop tracking RMSEs with pseudorange rates versus SGP4 errors.

If both pseudoranges and pseudorange rates are extracted by the receiver tracking the LEO SV, $\boldsymbol{z} = [\rho, \dot{\rho}]^{\mathsf{T}}$ and the measurement Jacobian $\mathbf{H}_{\rho,\dot{\rho}}$ is given by $\mathbf{H}_{\rho,\dot{\rho}} = \begin{bmatrix}\mathbf{H}_{\rho}^{\mathsf{T}} & \mathbf{H}_{\dot{\rho}}^{\mathsf{T}}\end{bmatrix}^{\mathsf{T}}$.

Figs. 3–5 show the SGP4 position and velocity errors in the SV's body frame RMSE versus the EKF closed-loop tracking RMSEs with pseudorange, pseudorange rate, and fused pseudorange and pseudorange rate measurements, respectively. It can be seen that the cross-track direction is the least observable for both position and velocity states. This can be explained by the fact that the SV's motion is in the along-track–radial plane, which is known as the orbital plane. As a result, the cross-track direction is not excited during the SV's motion, which leads to poor estimability of the corresponding states. Furthermore, it can be observed that the along-track position and radial velocity states are more observable than the along-track velocity and radial position states for this SV's trajectory relative to the tracking receiver.

Fig. 6 shows the magnitude of the position RMSE for the SGP4-propagated SV's states as well as the closed-loop tracked ephemeris using pseudoranges, pseudorange rates, and fused pseudoranges and pseudorange rates. It

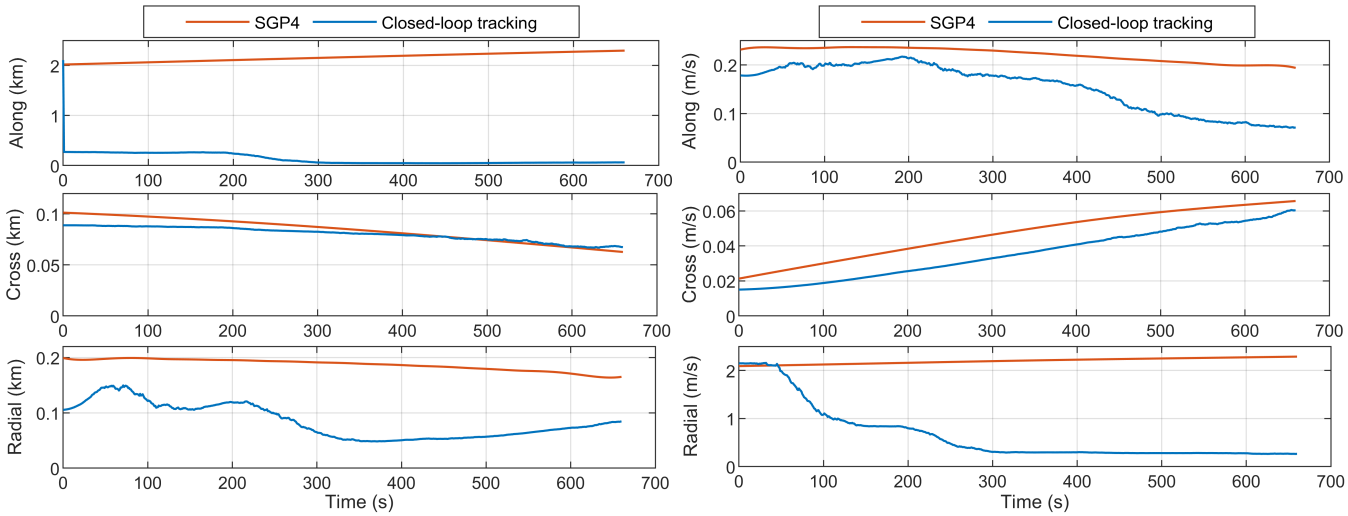

Fig. 5. LEO SV position and velocity closed-loop tracking RMSEs with fused pseudoranges and pseudorange rates versus SGP4 errors.

can be seen that if only one type of measurement is available, a receiver extracting pseudoranges has a better tracking performance than a receiver extracting pseudorange rates. Furthermore, fusing both pseudoranges and pseudorange rates yields negligible improvements over pseudorange-only tracking. This is suggested by the fact that both types of measurements are highly correlated, thus leading to a negligible information increase when augmenting the pseudorange measurement vector to include both navigation observables.

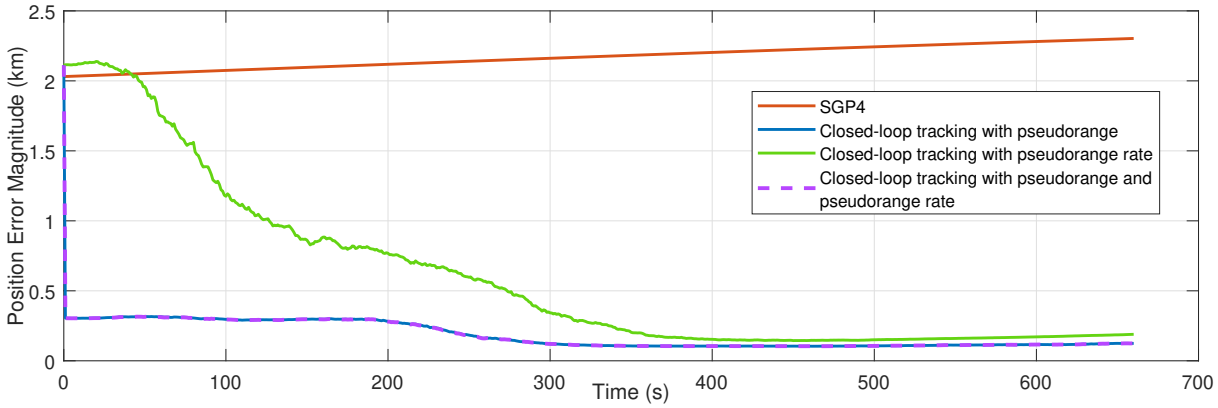

Fig. 6. LEO SV position RMSE magnitude with open-loop SGP4 versus closed-loop tracking with (i) pseudorange, (ii) pseudorange rate, and (iii) fused pseudorange and pseudorange rate.

IV. SIMULATION RESULTS: RECEIVER LOCALIZATION

To demonstrate the practical benefits of the refined LEO SV ephemeris, stationary receiver localization is performed in simulations. The localization is achieved via a batch least squares estimator using measurements drawn by an unknown receiver to two LEO SVs from the moment the SVs are visible to the receiver until the moment when this line-of-sight access is lost. This receiver localization will be performed: (i) using the LEO SVs' ground truth STK ephemeris, (ii) using the LEO SVs' ephemeris given by propagating with SGP4 the associated SVs' TLE, and (iii) using the ephemeris refined by the closed-loop tracking of the SVs by a known receiver that would transmit this information to the unknown receiver to be localized. The results of these three cases will be compared to assess the impact of the closed-loop tracking of LEO SVs on the localization accuracy.

The state vector $\boldsymbol{x} \triangleq \left[\boldsymbol{r}_r^{\mathsf{T}}, c\Delta\delta t_{\mathrm{SV}_1}, c\Delta\dot{\delta} t_{\mathrm{SV}_1}, c\Delta\delta t_{\mathrm{SV}_2}, c\Delta\dot{\delta} t_{\mathrm{SV}_2}\right]^{\mathsf{T}}$ is estimated by the batch nonlinear least squares (NLS), where $\boldsymbol{r}_r$ is the position of the unknown receiver in an Earth-centered, Earth-fixed (ECEF) reference frame.

This ECEF frame is chosen over the ECI frame where the LEO SV tracking was performed so that the receiver coordinates do not change over the batch window as the Earth rotates. As such, the LEO SVs' ephemerides are also computed in the ECEF frame from their ECI counterparts by accounting for Earth's rotation, nutation and precession effects, and polar motion. The measurements used in the NLS are the time history of the pseudoranges drawn by the unknown receiver to both LEO SVs $\boldsymbol{z} = \left[\boldsymbol{z}_1^\mathsf{T}, \boldsymbol{z}_2^\mathsf{T}\right]^\mathsf{T}$, where $\boldsymbol{z}_i = [\rho_i(1), \rho_i(2), \ldots, \rho_i(N_i)]^\mathsf{T}, i = 1, 2$, with N_i being the number of measurements drawn at a rate of 1 Hz over the visibility period of the i^{th} SV. Both the difference in clock bias and drift between the receiver and each SV are estimated, effectively casting the time evolution of the relative clock bias term present in (4) as a first-order polynomial.

The measurement equation $\boldsymbol{z} = \boldsymbol{g}(\boldsymbol{x})$ is first linearized about the current estimate $\hat{\boldsymbol{x}}$ to obtain $\Delta\boldsymbol{z} = \mathbf{G}\Delta\boldsymbol{x}$, where $\Delta\boldsymbol{z} = \boldsymbol{z} - \boldsymbol{g}(\hat{\boldsymbol{x}})$ and $\Delta\boldsymbol{x} = \boldsymbol{x} - \hat{\boldsymbol{x}}$. Then, the least squares solution to the set of linearized equation is found by $\Delta\boldsymbol{x} = \left(\mathbf{G}^\mathsf{T}\mathbf{G}\right)^{-1}\mathbf{G}^\mathsf{T}\Delta\boldsymbol{z}$. Finally, the state estimate $\hat{\boldsymbol{x}}$ is iteratively updated using $\hat{\boldsymbol{x}} = \hat{\boldsymbol{x}} + \Delta\boldsymbol{x}$ until convergence. Here, $\mathbf{G} \triangleq \begin{bmatrix}\mathbf{G}_1^\mathsf{T} & \mathbf{G}_2^\mathsf{T}\end{bmatrix}^\mathsf{T}$, $\boldsymbol{h}_{\text{sv}_i}(n_i) \triangleq \frac{\left[\hat{\boldsymbol{r}}_r - \boldsymbol{r}_{\text{sv}_i}(n_i)\right]}{\left\|\hat{\boldsymbol{r}}_r - \boldsymbol{r}_{\text{sv}_i}(n_i)\right\|_2}$, $i = 1, 2$ and $n_i = 1, 2, \ldots, N_i$, where

$$\mathbf{G_1} \triangleq \begin{bmatrix} \boldsymbol{h}_{\text{sv}_1}^\mathsf{T}(1) & 1 & 0 & \mathbf{0}_{1\times 2} \\ \boldsymbol{h}_{\text{sv}_1}^\mathsf{T}(2) & 1 & 1 & \mathbf{0}_{1\times 2} \\ \vdots & \vdots & \vdots & \vdots \\ \boldsymbol{h}_{\text{sv}_1}^\mathsf{T}(N_1) & 1 & N_1 - 1 & \mathbf{0}_{1\times 2} \end{bmatrix}, \quad \mathbf{G_2} \triangleq \begin{bmatrix} \boldsymbol{h}_{\text{sv}_2}^\mathsf{T}(1) & \mathbf{0}_{1\times 2} & 1 & 0 \\ \boldsymbol{h}_{\text{sv}_2}^\mathsf{T}(2) & \mathbf{0}_{1\times 2} & 1 & 1 \\ \vdots & \vdots & \vdots & \vdots \\ \boldsymbol{h}_{\text{sv}_2}^\mathsf{T}(N_2) & \mathbf{0}_{1\times 2} & 1 & N_2 - 1 \end{bmatrix}.$$

The localization of the unknown receiver using the tracked LEO SVs' ephemerides will be performed for each of the Monte Carlo realizations of subsection III-B and the localization error will be averaged over all Monte Carlo runs. This averaged localization error for the tracked ephemerides of the closed-loop filter as well as the localization errors computed using the SVs' ground truth orbits extracted from STK and the SGP4-propagated ephemerides are summarized in Table I.

TABLE I

Simulation results for unknown receiver localization with pseudorange measurements from two Orbcomm LEO SVs.

	STK ground truth	**SGP4 ephemerides**	**Closed-loop ephemerides**
Localization error (m)	9.5	2,187.4	249.7

V. EXPERIMENTAL RESULTS

In this section, experimental results are presented to demonstrate the refinement of the SGP4-propagated ephemerides of two Orbcomm LEO SVs tracked using carrier phase navigation observables drawn to a known receiver onboard a navigating UAV. Then, the localization performances of an unknown stationary receiver extracting carrier phase navigation observables from the Orbcomm SVs' signals are compared for three different SVs' ephemerides fed into the NLS: (i) positions and velocities obtained from the GPS-mounted receivers onboard the Orbcomm SVs, (ii) SGP4-propagated positions and velocities, and (iii) the refined positions and velocities tracked by the UAV. The carrier phase navigation observables for both SV tracking and receiver localization were corrected for ionospheric and tropospheric delays using models from [42]. Additionally, only measurements recorded for SV elevations greater than 10° were filtered for both LEO SV tracking and unknown stationary receiver localization.

Fig. 7 show the along-track, cross-track, and radial position states' SGP4 errors in addition to the EKF errors with their associated sigma bounds for Orbcomm FM108 and FM106 SVs, respectively. It can be seen that the along-track position state, where most of the SV's position error lies, is observable for both SVs with decreasing errors and reduced uncertainties. It is also worth noting that the radial position state is more observable for Orbcomm FM116 SV than for Orbcomm FM108 SV. This can be explained by the fact that SV FM116's motion relative to the tracking receiver excites the radial direction while SV FM108's trajectory does not as shown in the sky plot of Fig. 8.

The EKF tracking of the two Orbcomm satellites results in refined ephemerides for both FM108 and FM116 SVs as shown in Fig. 7. This refined tracking is materialized by a position RMSE across the SV's visibility period of 436.3 m and 441.5 m for FM108 and FM116 SVs respectively, improving on SGP4's 1,073.4 m RMSE. Moreover, the

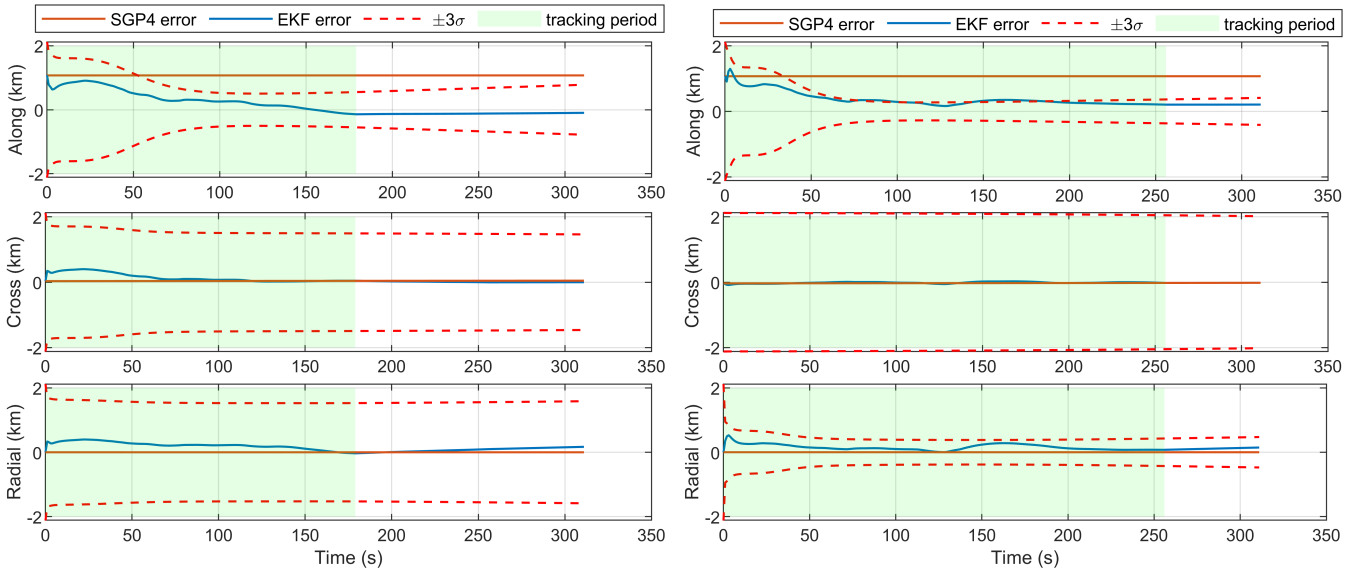

Fig. 7. Orbcomm FM108 (left) and Orbcomm FM116 (right) EKF-tracked position errors with associated sigma bounds versus open-loop SGP4 errors.

last position estimate error computed by the tracking receiver reduced by 879.3 m and 817.7 m the position error computed from SGP4's open-loop propagations for FM108 and FM106 SVs respectively.

For the unknown stationary receiver localization experimental application, the NLS was initialized with a receiver position 1,047 km away from the actual receiver position. The final 2-D localization results using (i) GPS-transmitted ephemerides, (ii) SGP4-propagated ephemerides, and (iii) EKF-tracked ephemerides of the two Orbcomm SVs are shown in Fig. 8 and are summarized in Table II. These large localization errors compared to that of Section IV are explained by the fact that for the experiment, the relative clock bias term is estimated to be constant over the satellite visibility, thus leading to a model mismatch; while in simulations, the time evolution of this term was estimated to be a first-order polynomial (both bias and drift were estimated). It was seen that estimating both the relative bias and drift yielded worse localization performance than only estimating a constant bias for the experiment. This is suspected to be caused by the poor receiver–SVs geometry shown in the sky plot of Fig. 8, but further investigation needs to be conducted on this topic.

TABLE II

Experimental results for unknown receiver localization with carrier phase measurements from two Orbcomm LEO SVs.

	GPS-transmitted ephemerides	**SGP4 ephemerides**	**Closed-loop ephemerides**
Localization error (m)	498	1,687	782

VI. CONCLUSION

This paper proposed a framework to perform closed-loop tracking of LEO SVs using navigation observables drawn from their signals. The overarching goal is to refine the LEO SVs' ephemerides in order to improve the localization performance of an unknown receiver. A Monte Carlo analysis was run to determine the process noise covariance matrix which was then characterized in the SV's body frame for better generalization. Closed-loop tracking of LEO SVs via an EKF was performed using (i) pseudoranges, (ii) pseudorange rates, and (iii) fused pseudoranges and pseudorange rates in simulations and reduced errors were achieved compared to the open-loop SGP4 propagations. The refined ephemerides were also reflected in improved localization of an unknown receiver. Finally, both SV ephemeris tracking and unknown receiver localization were demonstrated experimentally with a reduction of 879.3 m and 817.7 m in position error for two Orbcomm LEO SVs for LEO ephemerides tracking and a 53.65% reduction in the receiver 2-D localization error.

Fig. 8. Experimental results showing (a) the initialization of the NLS, (b) the sky plot of Orbcomm FM108 and FM116 SVs during the experiment, and (c) the final 2-D stationary receiver localization errors using (i) GPS-transmitted ephemerides, (ii) SGP4-propagated ephemerides, and (iii) closed-loop tracked ephemerides. Map data: Google Earth.

Acknowledgment

This work was supported in part by the Office of Naval Research (ONR) under Grant N00014-19-1-2511 and Grant N00014-19-1-2613 and in part by the National Science Foundation (NSF) under Grant 1929965. The authors would like to thank Analytical Graphics, Inc. (AGI) for making Systems Tool Kit (STK) available for research purposes.

References

[1] L. Boldt-Christmas, "Low Earth orbit," http://www.esa.int/ESA_Multimedia/Images/2020/03/Low_Earth_orbit, March 2020.
[2] M. Harris, "Tech giants race to build orbital internet [news]," *IEEE Spectrum*, vol. 55, no. 6, pp. 10–11, 2018.
[3] N.Okati, T. Riihonen, D. Korpi, I. Angervuori, and R. Wichman, "Downlink coverage and rate analysis of low earth orbit satellite constellations using stochastic geometry," *IEEE Transactions on Communications*, vol. 68, no. 8, pp. 5120–5134, August 2020.
[4] H. Curtis, *Orbital mechanics for engineering students*, 4th ed. Butterworth-Heinemann, 2019.
[5] T. Reid, B. Chan, A. Goel, K. Gunning, B. Manning, J. Martin, A. Neish, A. Perkins, and P. Tarantino, "Satellite navigation for the age of autonomy," in *Proceedings of IEEE/ION Position, Location and Navigation Symposium*, 2020, pp. 342–352.
[6] T. Reid, K. Gunning, A. Perkins, S. Lo, and T. Walter, "Going back for the future: Large/mega LEO constellations for navigation," in *Proceedings of ION GNSS Conference*, September 2019, pp. 2452–2468.
[7] P. Iannucci and T. Humphreys, "Economical fused LEO GNSS," in *Proceedings of IEEE/ION Position, Location and Navigation Symposium*, 2020, pp. 426–443.
[8] J. Brodkin, "SpaceX says 12,000 satellites isn't enough, so it might launch another 30,000," https://arstechnica.com/information-technology/2019/10/spacex-might-launch-another-30000-broadband-satellites-for-42000-total, October 2019.
[9] A. Boley and M. Byers, "Satellite mega-constellations create risks in Low Earth Orbit, the atmosphere and on Earth," *Scientific Reports*, vol. 11, no. 1, pp. 1–8, 2021.
[10] G. Ritchie and T. Seal, "Why low-Earth orbit satellites are the new space race," https://www.washingtonpost.com/business/why-low-earth-orbit-satellites-are-the-new-space-race/2020/07/10/51ef1ff8-c2bb-11ea-8908-68a2b9eae9e0_story.html, July 2020.
[11] T. Reid, "Orbital diversity of global navigation satellite systems," Ph.D. dissertation, Stanford University, USA, 2017.
[12] D. Lawrence, H. Cobb, G. Gutt, M. OConnor, T. Reid, T. Walter, and D. Whelan, "Navigation from LEO: Current capability and future promise," *GPS World Magazine*, vol. 28, no. 7, pp. 42–48, July 2017.
[13] North American Aerospace Defense Command (NORAD), "Two-line element sets," http://celestrak.com/NORAD/elements/.
[14] D. Vallado and P. Crawford, "SGP4 orbit determination," in *Proceedings of AIAA/AAS Astrodynamics Specialist Conference and Exhibit*, August 2008, pp. 6770–6799.
[15] R. Landry, A. Nguyen, H. Rasaee, A. Amrhar, X. Fang, and H. Benzerrouk, "Iridium Next LEO satellites as an alternative PNT in GNSS denied environments–part 1," *Inside GNSS Magazine*, vol. 14, no. 3, pp. 56–64., May 2019.
[16] J. Khalife and Z. Kassas, "Receiver design for Doppler positioning with LEO satellites," in *Proceedings of IEEE International Conference on Acoustics, Speech and Signal Processing*, May 2019, pp. 5506–5510.
[17] F. Farhangian and R. Landry, "Multi-constellation software-defined receiver for Doppler positioning with LEO satellites," *Sensors*, vol. 20, no. 20, pp. 5866–5883, October 2020.
[18] Z. Tan, H. Qin, L. Cong, and C. Zhao, "New method for positioning using IRIDIUM satellite signals of opportunity," *IEEE Access*, vol. 7, pp. 83 412–83 423, 2019.
[19] M. Orabi, J. Khalife, and Z. Kassas, "Opportunistic navigation with Doppler measurements from Iridium Next and Orbcomm LEO satellites," in *Proceedings of IEEE Aerospace Conference*, March 2021, pp. 1–9.
[20] M. Psiaki, "Navigation using carrier doppler shift from a LEO constellation: TRANSIT on steroids," *NAVIGATION, Journal of the Institute of Navigation*, vol. 68, no. 3, pp. 621–641, September 2021.

[21] M. Neinavaie, J. Khalife, and Z. Kassas, "Blind opportunistic navigation: Cognitive deciphering of partially known signals of opportunity," in *Proceedings of ION GNSS Conference*, September 2020, pp. 2748–2757.
[22] J. Khalife, M. Neinavaie, and Z. Kassas, "Blind Doppler tracking from OFDM signals transmitted by broadband LEO satellites," in *Proceedings of IEEE Vehicular Technology Conference*, April 2021, pp. 1–6.
[23] M. Neinavaie, J. Khalife, and Z. Kassas, "Blind Doppler tracking and beacon detection for opportunistic navigation with LEO satellite signals," in *Proceedings of IEEE Aerospace Conference*, March 2021, pp. 1–8.
[24] M. Neinavaie, J. Khalife, and Z. Kassas, "Exploiting Starlink signals for navigation: first results," in *Proceedings of ION GNSS Conference*, September 2021, accepted.
[25] J. Khalife, M. Neinavaie, and Z. Kassas, "The first carrier phase tracking and positioning results with Starlink LEO satellite signals," *IEEE Transactions on Aerospace and Electronic Systems*, 2021, accepted.
[26] Systems Tool Kit (STK), "High-Precision Orbit Propagator (HPOP)," https://help.agi.com/stk/11.0.1/Content/hpop/hpop.htm, September 2016.
[27] A. Rich, "Investigating analytical and numerical methods to predict satellite orbits using two-line element sets," Master's thesis, Air Force Institute of Technology, Wright-Patterson Air Force Base, Ohio, USA, 2017.
[28] Z. Yang, Y. Luo, V. Lappas, and A. Tsourdos, "Nonlinear analytical uncertainty propagation for relative motion near $j2$-perturbed elliptic orbits," *Journal of Guidance, Control, and Dynamics*, vol. 43, no. 4, pp. 888–903, April 2018.
[29] H. Peng and X. Bai, "Artificial neural network–based machine learning approach to improve orbit prediction accuracy," *Journal of Spacecraft and Rockets*, vol. 55, no. 5, pp. 1248–1260, 2018.
[30] H. Peng and X. Bai, "Comparative evaluation of three machine learning algorithms on improving orbit prediction accuracy," *Astrodynamics*, vol. 3, no. 4, pp. 325–343, 2019.
[31] D. Shen, J. Lu, G. Chen, E. Blasch, C. Sheaff, M. Pugh, and K. Pham, "Methods of machine learning for space object pattern classification," in *Proceedings of IEEE National Aerospace and Electronics Conference*, 2019, pp. 565–572.
[32] B. Li, J. Huang, Y. Feng, F. Wang, and J. Sang, "A machine learning-based approach for improved orbit predictions of LEO space debris with sparse tracking data from a single station," *IEEE Transactions on Aerospace and Electronic Systems*, vol. 56, no. 6, pp. 4253–4268, 2020.
[33] Z. Kassas, J. Morales, and J. Khalife, "New-age satellite-based navigation – STAN: simultaneous tracking and navigation with LEO satellite signals," *Inside GNSS Magazine*, vol. 14, no. 4, pp. 56–65, 2019.
[34] Z. Kassas, J. Khalife, M. Neinavaie, and T. Mortlock, "Opportunity comes knocking: overcoming GPS vulnerabilities with other satellites' signals," *Inside Unmanned Systems Magazine*, pp. 30–35, June/July 2020.
[35] T. Mortlock and Z. Kassas, "Performance analysis of simultaneous tracking and navigation with LEO satellites," in *Proceedings of ION GNSS Conference*, September 2020, pp. 2416–2429.
[36] S. Kozhaya, J. Haidar-Ahmad, A. Abdallah, S. Saab, and Z. Kassas, "Comparison of neural network architectures for simultaneous tracking and navigation with LEO satellites," in *Proceedings of ION GNSS Conference*, September 2021, accepted.
[37] J. Vetter, "Fifty years of orbit determination: Development of modern astrodynamics methods," *Johns Hopkins APL Technical Digest*, vol. 27, no. 3, pp. 239–252, November 2007.
[38] O. Montenbruck and E. Gill, *Satellite orbits: models, methods, and applications*. Springer, 2000.
[39] B. Tapley, M. Watkins, C. Ries, W. Davis, R. Eanes, S. Poole, H. Rim, B. Schutz, C. Shum, R. Nerem, F. Lerch, J. Marshall, S. Klosko, N. Pavlis, and R. Williamson, "The Joint Gravity Model 3," *Journal of Geophysical Research*, vol. 101, no. B12, pp. 28 029–28 049, December 1996.
[40] J. Vinti, *Orbital and Celestial Mechanics*. American Institute of Aeronautics and Astronautics, 1998.
[41] Analytical Graphics, Inc, "Systems Tool Kit (STK)," https://www.agi.com/getmedia/172b0f02-7469-4fbf-9d5c-9c6e6f36aa87/STK-Pro-Product-Specsheet.pdf?ext=.pdf), April 2020.
[42] P. Misra and P. Enge, *Global Positioning System: Signals, Measurements, and Performance*, 2nd ed. Ganga-Jamuna Press, 2010.